


Article

Facile Synthesis, Characterization, and Photocatalytic Performance of BiOF/BiFeO₃ Hybrid Heterojunction for Benzylamine Coupling under Simulated Light Irradiation

Abdalla S. Abdelhamid ^{1,2}, Reem H. Alzard ¹, Lamia A. Siddig ¹, Aya Elbahnasy ¹, Duha Aljazmati ¹, Zaina Kadoura ¹, Hind Zeidane ¹, Rufaida Elshikh ¹ and Ahmed Alzamly ^{1,*} 

¹ Department of Chemistry, United Arab Emirates University, Al-Ain P.O. Box 15551, United Arab Emirates

² Department of Chemical Engineering, United Arab Emirates University, Al-Ain P.O. Box 15551, United Arab Emirates

* Correspondence: ahmed.alzamly@uaeu.ac.ae

Abstract: Under simulated light irradiation, the aerobic oxidation of benzylamine to *N,N*-benzylidene benzylamine was carried out as a model reaction to investigate the photocatalytic activity of a hydrothermally prepared composite based on BiOF and BiFeO₃ materials. The prepared photocatalysts were characterized using several spectroscopic techniques, such as powder X-ray diffraction (PXRD), diffuse reflectance spectroscopy (DRS), scanning electron microscopy (SEM), energy-dispersive X-ray spectroscopy (EDX), and Fourier transform infrared spectroscopy (FTIR). Band gap analysis showed that the composite exhibits a band gap that lies in the UV region (3.5 eV). Nonetheless, pristine BiOF and BiFeO₃ exhibited band gaps of 3.8 eV and 2.15 eV, respectively. *N,N*-benzylidenebenzylamine was selectively achieved with a high conversion yield of ~80% under atmospheric conditions in which the product was confirmed using ¹H-NMR, ¹³C-NMR, and FTIR spectroscopic techniques. Various control experiments were conducted to further confirm the enhanced photocatalytic performance of the reported composite.

Keywords: photocatalyst; simulated light; band gap; hybrid heterojunction; benzylamine



Citation: Abdelhamid, A.S.; Alzard, R.H.; Siddig, L.A.; Elbahnasy, A.; Aljazmati, D.; Kadoura, Z.; Zeidane, H.; Elshikh, R.; Alzamly, A. Facile Synthesis, Characterization, and Photocatalytic Performance of BiOF/BiFeO₃ Hybrid Heterojunction for Benzylamine Coupling under Simulated Light Irradiation.

Photochem **2023**, *3*, 187–196. <https://doi.org/10.3390/photochem3010012>

Academic Editor: Vincenzo Vaiano

Received: 5 February 2023

Revised: 10 March 2023

Accepted: 14 March 2023

Published: 21 March 2023



Copyright: © 2023 by the authors. Licensee MDPI, Basel, Switzerland. This article is an open access article distributed under the terms and conditions of the Creative Commons Attribution (CC BY) license (<https://creativecommons.org/licenses/by/4.0/>).

1. Introduction

Since its discovery in 1960, bismuth ferrite has garnered considerable interest due to its rarity as one of the few multiferroics with the simultaneous presence of ferroelectric and antiferromagnetic order characteristics in a perovskite structure [1,2]. An inorganic semiconductor, bismuth ferrite (BiFeO₃, BFO) is a promising multifunctional material with a wide range of intriguing applications, including spintronics [3,4], sensors [5,6], photocatalysis [7–9], optical devices [10,11], and data storage [12]. Due to the narrow band gap energy of BFO and the potential for internal polarization suppression of the electron–hole recombination rate, it has unique advantages as a heterogenous photocatalyst [13,14]. Compared to the commonly used TiO₂ photocatalyst [15], which absorbs in the UV region due to its broad band gap, BFO narrow band gap enables the greatest and most efficient exploitation of visible light from solar radiation energy [16,17]. In photocatalytic applications, the behavior of BFO in the presence of visible light is of particular interest due to the number of distinctive properties it holds, including a low cost [18], nontoxicity [19,20], chemical stability [18], discrete crystalline structure [18], and special electro-optical properties [21].

BFO perovskites can only stabilize over a limited range of temperatures, and, until now, the problem of obtaining single-phase pure BFO crystallite remains challenging. Nonetheless [8], a range of wet chemical techniques have been employed to create pure single-phase BiFeO₃. A hydrothermal procedure can create pure single-phase BiFeO₃ at low temperatures, but pressure is necessary [22]. These procedures include the microemulsion

technique [23], the ferrioxalate precursor method [24], the solution combustion method [25], and the citrate method [26], and using sol-gel techniques based on ethylene glycol [27].

It has been proven in many previous studies that metal-oxides-based photocatalysts perform better when heterojunctions are formed; thus, attention to the assembly of various heterojunction structures has grown in the past few years. For example, heterojunctions such as BiOF/BiOI [28], MoS₂/BiVO₄ [29], BiOI/TiO₂ [30], NiS/CdS [31], and SnO₂/TiO₂ [32] were used as photocatalysts for the removal of diclofenac potassium, the photodegradation of methylene blue, the photodegradation of methyl orange, photocatalytic H₂-production, and the decolorization of rhodamine-B, respectively.

In this study, the coprecipitation method was used to generate pure single-phase BFO crystallites at a low temperature of about 70 °C. This method had the ability to create BFO powders that were well crystallized, had regulated morphology, and had a limited dispersion of particle size. Notably, all previous studies on BFO materials have focused on magnetic and dielectric properties. Nevertheless, our present study focuses on the photocatalytic aspect of this material and a newly prepared heterojunction based on BiFeO₃ and BiOF. The photocatalytic activity has been investigated using the photocatalytic benzyl amine coupling reaction as a model reaction.

2. Experimental

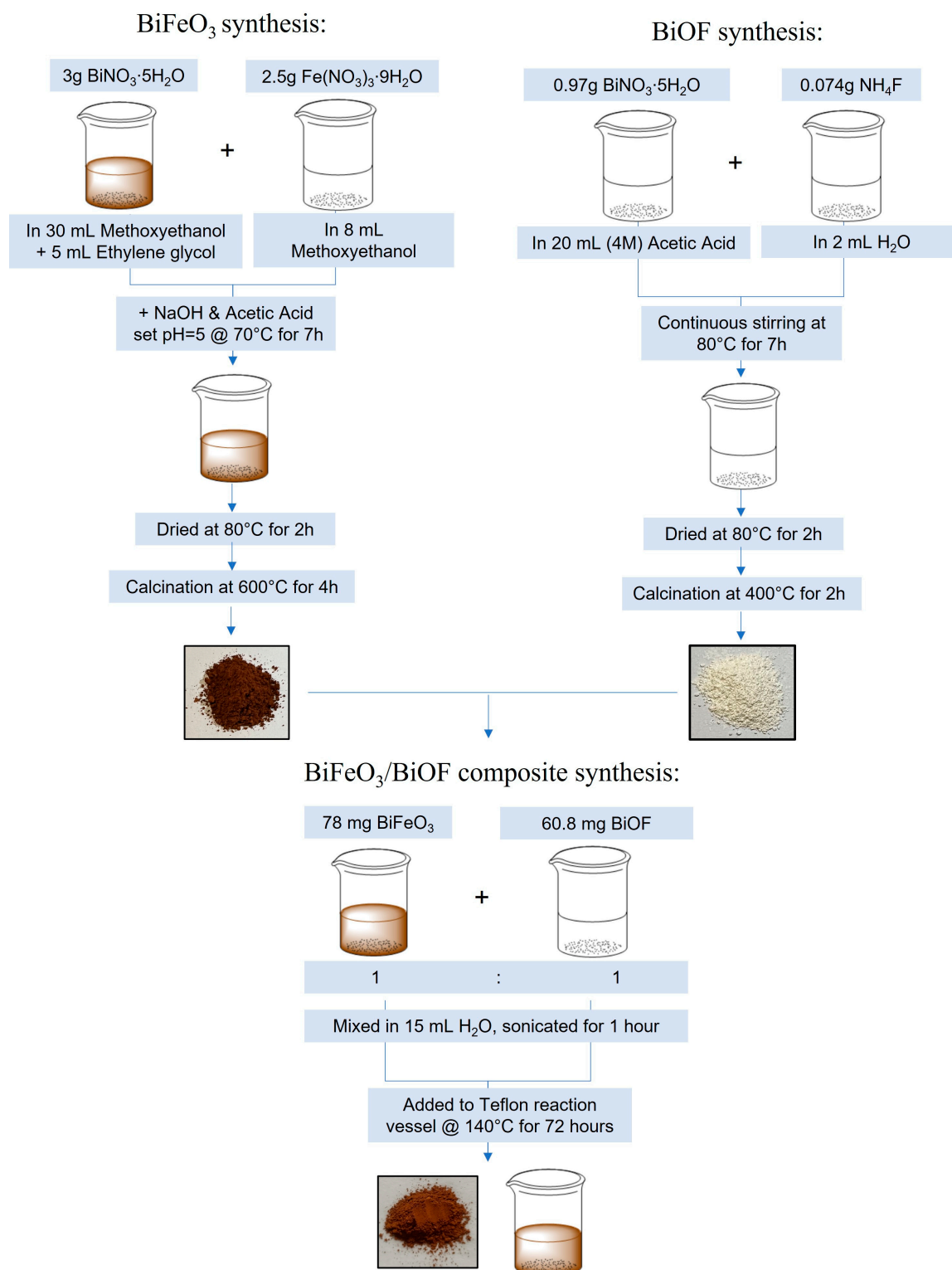
2.1. Materials and General Procedures

Bismuth nitrate pentahydrate (BiNO₃·5H₂O), iron nitrate nonahydrate (Fe(NO₃)₃·9H₂O), ammonium fluoride (NH₄F), deuterated chloroform (CDCl₃), acetonitrile (CH₃CN, ACN), glacial acetic acid (CH₃COOH), and benzylamine (C₇H₉N) were purchased from Sigma-Aldrich (St. Louis Missouri, MO, USA) and used as received. The FTIR spectrum was obtained using ATR-IR spectroscopy (Agilent Technologies Cary 600 Series FTIR Spectrometer, Santa Clara, CA, USA) across a range of 4000 to 500 cm⁻¹ (512 scan average), in which the background was first collected using potassium bromide where the oily product was sandwiched between two KBr disks. Using a benchtop Rigaku MiniFlex X-ray diffractometer (Neu-Isenburg, Germany) with a CuKα radiation tube (λ = 1.542 Å) operating at 40 kV across a range of 3–50° (2θ) and a rate of 2 °C min⁻¹, powder X-ray diffraction (PXRD) (Neu-Isenburg, Germany) measurements were made. The sample surface morphology and elemental analysis were analyzed using Quattro ESEM instrument scanning electron microscopy (SEM) (Waltham, MA, USA), equipped with an energy-dispersive X-ray (EDX) detector, that was operated at high vacuum with 30 kV accelerating voltage. Diffuse reflectance (DRS) of BiFeO₃, BiOF, and the composite was measured using a Shimadzu UV-3600 spectrophotometer (Kyoto, Japan) over wavelength ranges from 200 nm to 800 nm after a baseline measurement using barium sulfate. Proton nuclear magnetic resonance, ¹H-NMR, and ¹³C-NMR spectra were acquired using a Varian 400 MHz (Palo Alto, CA, USA) in d-chloroform as the solvent to validate the identity of the product. Nitrogen sorption experiments at 77 K were used to assess the surface area and porosity of the photocatalysts.

2.2. Preparation of the Photocatalysts

2.2.1. Preparation of BiFeO₃

Bismuth ferrite was synthesized using the coprecipitation method. Bismuth nitrate and iron nitrate were dissolved separately in 2-methoxyethanol and left under stirring until completely dissolved. In detail, 6.18 × 10⁻³ moles of bismuth nitrate and iron nitrate equivalent to 3 g and 2.5 g were used, respectively. A total of 30 mL of 2-methoxyethanol was used to dissolve bismuth nitrate and an additional 5 mL of ethylene glycol was added to enhance the solubility of bismuth nitrate. For iron nitrate, 8 mL of 2-methoxyethanol was needed. The two solutions were mixed, and the pH was set to 5 using acetic acid and ammonium hydroxide. The solution was then left under continuous stirring and heating at 70 °C for around 7 h. The product was then collected and washed with DI water and ethanol several times. It was subsequently dried for 2 h at 80 °C, then calcined at 600 °C for 4 h (Scheme 1).



Scheme 1. Schematic syntheses of the hydrothermal method for preparing BiFeO₃, BiOF, and BiOF/BiFeO₃ composite using hydrothermal methods.

2.2.2. Preparation of BiOF

According to previously reported procedure, BiOF was synthesized using simple coprecipitation method [28]. Bismuth nitrate and ammonium fluoride were utilized in quantities of 0.002 mols each, or 970 mg and 74.08 mg, respectively. Bismuth nitrate was dissolved in 20 mL of 4 M acetic acid with constant stirring and heating at 80 °C. Then,

ammonium fluoride was dissolved in 2 mL of deionized water (DI) and added to bismuth nitrate solution. The mixture was left under continuous stirring and heating at 80 °C for 7 h. The product was then collected and washed with DI water and ethanol several times. It was subsequently dried for 2 h at 80 °C and calcined for 4 h at 400 °C (Scheme 1).

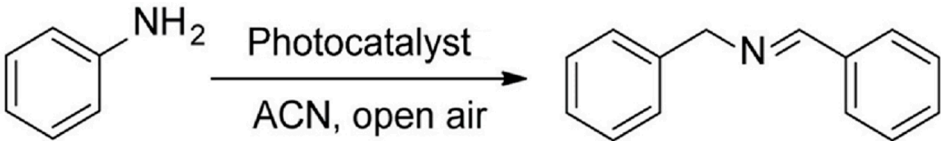
2.2.3. Preparation of BiFeO₃/BiOF Composite

BiFeO₃/BiOF composite was synthesized using the simple hydrothermal method. A molar ratio of 1:1 was used from each of BiFeO₃ and BiOF, which was added to a 25 mL Teflon line autoclave with 15 mL of DI water. The mixture was sonicated for 1 h before heating at 140 °C for 72 h (Scheme 1).

2.2.4. Photocatalytic Activity

In a 25 mL round-bottom flask connected to a condenser, the photocatalytic reaction was conducted under aerobic conditions. An optimum of 5.0 mg (0.16, 0.02, 0.009 mmol for BiOF, BiFeO₃, and BiOF/BiFeO₃ composite, respectively) of each sample was added to 51 µL (0.50 mmol) of benzyl amine in 2 mL of acetonitrile (ACN). The reaction was then irradiated by a 400 W halogen lamp for 24 h. The photocatalysts were washed with ACN and separated from the product by syringe filtration. Product purification was completed by simple column chromatography using silica gel and a mixture of ethyl acetate and hexane (1:2) to remove any possible impurities or byproducts. To isolate the product (*N*-benzylidenebenzylamine) that was dissolved in ACN, the solvent was evaporated using a rotary evaporator. Finally, ¹H-NMR, ¹³C-NMR, and FTIR techniques were used to confirm the identity of the product. All control experiments followed the same procedure with required changes in some variables, as outlined in Table 1.

Table 1. Photocatalytic coupling of benzylamine to *N*-benzylidenebenzylamine over BiFeO₃, BiOF, and BiFeO₃/BiOF composite.

	
Photocatalyst	Conversion Yield (%)
BiFeO ₃	18
BiOF	39
BiOF/BiFeO ₃ composite	80

Reaction optimum conditions: 0.5 mmol (51 µL) benzylamine, and 0.160, 0.020, and 0.009 mmol (5 mg) of BiFeO₃, BiOF, and BiFeO₃/BiOF composite, respectively; open air; irradiated for 24 h.

3. Results and Discussion

3.1. Characterization of the Photocatalysts

The purity and phase structure of prepared BiFeO₃ and BiOF were confirmed by the PXRD diffraction pattern and compared to the standard PXRD database (JCPDS file No. 01-073-0548 and 73-1595 for BiFeO₃ and BiOF, respectively), as shown in Figures S1 and S2 in the Supporting Information. All diffraction peaks were matched using Match!3 software (version 3.0) to the pure trigonal and tetragonal phases of BiFeO₃ and BiOF, respectively, with no extra peaks determining any impurities the samples may contain. The BiOF diffraction peaks indexed to (001), (101), (002), (110), (102), (112), (200), (103), and (211), which showed at 2θ of 14.16°, 27.64°, 28.58°, 33.66°, 37.42°, 44.82°, 48.46°, 50.15°, and 56.77°, respectively. On the other hand, the BiFeO₃ diffraction peaks indexed to (002), (012), (110), (013), (004), (020), (114), and (122), which appeared at 2θ of 19.34°, 29.2°, 31.93°, 37.21°, 39.62°, 45.93°, 51.5°, and 55.56°, respectively. Moreover, upon comparing the PXRD pattern of the prepared photocatalyst BiOF/BiFeO₃ composite with both mixed metal

oxides (Figure 1), the obtained patterns showed a combination of similar peaks from both mixed materials, which confirmed the preparation of the composite.

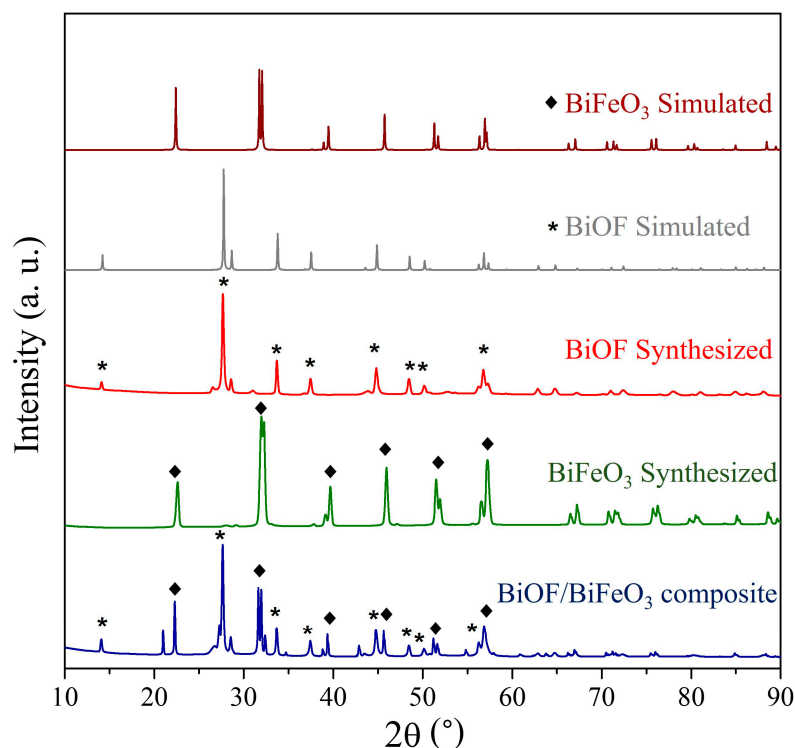


Figure 1. XRD patterns of the synthesized photocatalysts. BiFeO₃ is presented by (♦) and BiOF is presented by (*).

The band gaps of BiFeO₃, BiOF, and BiOF/BiFeO₃ composite were measured using the Tauc method [33], with which conduction band positions and band potential measurements could be estimated as previously reported [34,35]. When plotting ($\alpha h\nu$) vs. photon energy ($h\nu$), as shown in Figure 2, the BiFeO₃ exhibited a band of 2.15 eV lying in the visible region, and BiOF showed a larger band gap of 3.8 eV in the UV region. The BiOF/BiFeO₃ composite exhibited a band gap of 3.5 eV lying in the UV light region compared to pure BiOF, indicating that the synthesized composite forms a heterojunction interface.

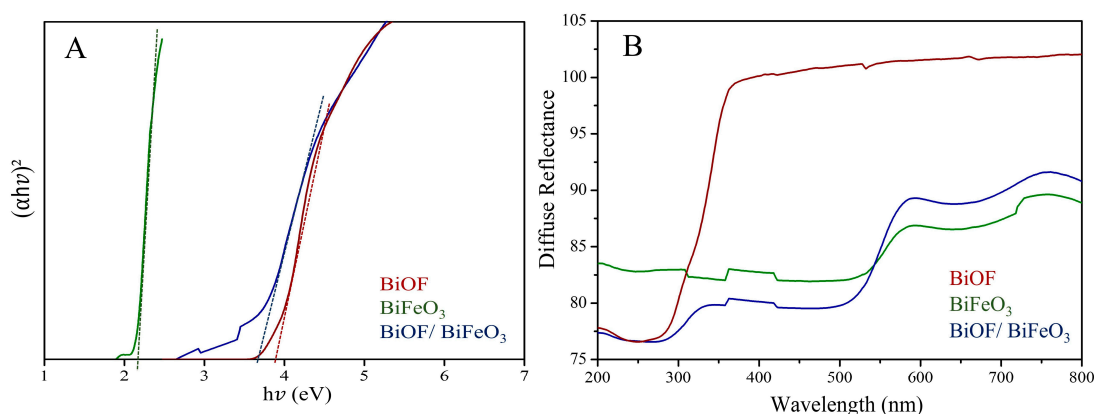


Figure 2. UV-Vis DRS spectra (A) and Tauc plots of prepared photocatalysts (B). The intercept at the x axis of the extended linear dashed lines in the graph determines the band gap values.

SEM images of pure BiFeO₃, BiOF, and composite BiOF/BiFeO₃ photocatalysts are shown in Figure 3. BiOF showed agglomerated small particles on an irregular surface, whereas BiFeO₃ possessed a spherical particle shape. As for the BiOF/BiFeO₃ compos-

ite, there is no specific adopted morphology from either material, but the composite has an irregular surface with agglomerated particles. The EDX data (Figures S3–S5, Supporting Information) were used to confirm the elemental composition of the synthesized photocatalyst. Atomic percent confirmed the presence of Bi, Fe, F, and O in the photocatalyst with a higher presence in Bi and O compared to both BiFeO_3 and BiOF (Tables S1–S3, Supporting Information).

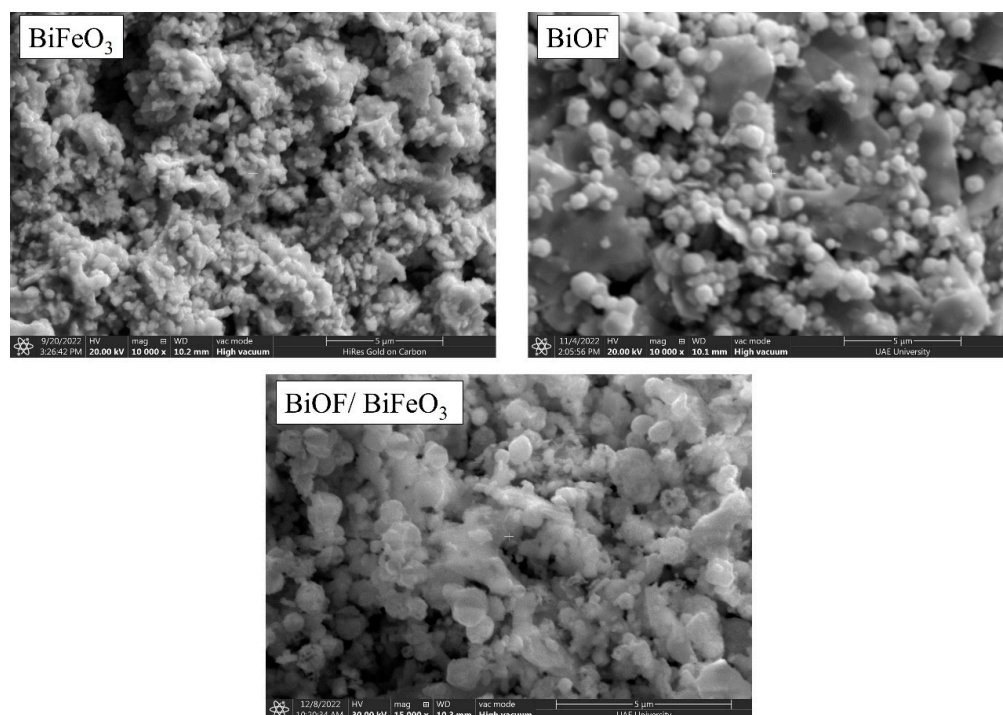


Figure 3. SEM images of the photocatalysts material at 5 μm scale bar.

The FT-IR spectra of the three materials are shown in Figure 4. FT-IR data were used to determine the bond present in the materials. BiFeO_3 has bands around 530, 550, and 750 cm^{-1} that represent the Fe–O stretching and bending vibrations. Bi–O/F vibrations in BiOF occurred at $415\text{--}558\text{ cm}^{-1}$. For the BiOF/BiFeO_3 composite, the 1405 cm^{-1} and 553 cm^{-1} bands are for the Bi–O and Fe–O bending and stretching bands, respectively.

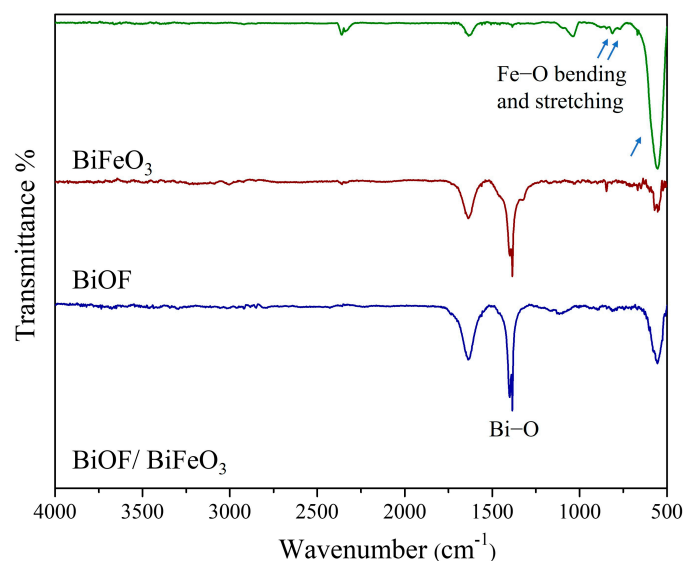


Figure 4. FTIR spectra of the prepared photocatalysts with corresponding band assignments.

3.2. Photocatalytic Activities

Based on their band gap values, the photocatalytic performance of the reported photocatalysts was tested using the photocatalytic oxidative coupling reaction of benzylamine as a model photocatalytic reaction. The photocatalytic experiments were carried out using 51 μL of benzyl amine placed in a 25 mL round-bottom flask irradiated from the side (10 cm from the radiation source) using light from a 400 W halogen lamp with a wavelength range of 340–850 nm. The round-bottom flask was attached to a condenser open at the top to the atmosphere. A pale-yellow oily product of *N*-benzylidenebenzylamine was formed and confirmed using ^1H -NMR and ^{13}C -NMR (Figure S6, Supporting Information). Peak shifts were as follows: ^1H -NMR (400 MHz, CDCl_3): δ 8.40 (s, 1H), 7.80–7.77 (m, 2H), 7.43–7.41 (m, 3H), 7.35–7.34 (m, 4H), 7.29–7.26 (m, 1H), 4.83 (s, 2H); ^{13}C -NMR (400 MHz, CDCl_3): δ 162, 139.23, 136.09, 130.78, 128.61, 128.49, 128.27, 127.98, 126.99, 65.06. Because of the newly appeared double bond formed after the coupling of another benzyl amine, the peak at 8.4 ppm was the most deshielded signal. The ^1H -NMR spectrum of the starting material benzyl amine was compared to the products in which the signal at 3.9 ppm ($-\text{CH}_2$ protons) was downfielded to 4.9 in *N*-benzylidenebenzylamine, which further confirms the coupling step. In agreement with this finding, ^{13}C -NMR data showed the highest shift at $\delta_{\text{C}} = 162$ ppm, which belongs to the characteristic peak of the $\text{N}=\text{C}$ bond of the products. Having the expected shifts along with the integration of each peak, the conversion percent yields using the three photocatalysts were calculated to be 18, 39, and 80% for BiFeO_3 , BiOF , and $\text{BiOF}/\text{BiFeO}_3$ composite, respectively, with no starting material or any other byproduct detected (Table 1). Due to rapid charge/hole recombination at lower band gaps, BiFeO_3 shows low conversion, while the composite had the highest conversion because the recombination was suppressed.

The enhanced yield of formation under UV light irradiation for the prepared $\text{BiOF}/\text{BiFeO}_3$ composite heterojunction in comparison to pure BiOF or BFO is mainly explained by the fact that a heterojunction formed by adding BiOF could absorb more photons and act as an efficient transfer of excited electrons from the BiOF conduction band to the conduction band of BFO particles; moreover, a transfer from the valence band of BiOF to the valence band of BFO suppresses recombination and allows greater electron transfer to benzyl amine.

To provide more evidence regarding the completion of the coupling reaction, FTIR spectra were recorded for the starting material and compared to the product as well. Upon coupling, the characteristic band of $-\text{NH}$ stretch in benzyl amine (3200 and 3500 cm^{-1}) disappeared, and a new band at 1643 cm^{-1} appeared, which corresponded to the $\text{C}=\text{N}$ of the product. Moreover, the bands of the benzene ring were obvious and appeared between 1650 and 1800 cm^{-1} (Figure S7, Supporting Information).

Different control experiments have been carried out to investigate other reaction conditions. As illustrated in Table 2, using the $\text{BiOF}/\text{BiFeO}_3$ composite photocatalyst showed the highest conversion. The percent yields were calculated as previously reported [33]. The highest yields of *N*-benzylidenebenzylamine products were obtained in an open-air and acetonitrile environment, while 0, 7, and 13% were obtained using BiFeO_3 , BiOF , and $\text{BiOF}/\text{BiFeO}_3$ composite, respectively, in a solvent-free condition (Entries II–IV), which confirms that our photocatalysts work best in the solvent environment. Many other control experiments have shown no conversion yields in the absence of either light (Entries V–VII) or photocatalysts (entries VIII), which strongly supports the high photocatalytic activity of the reported photocatalysts under visible or UV irradiation.

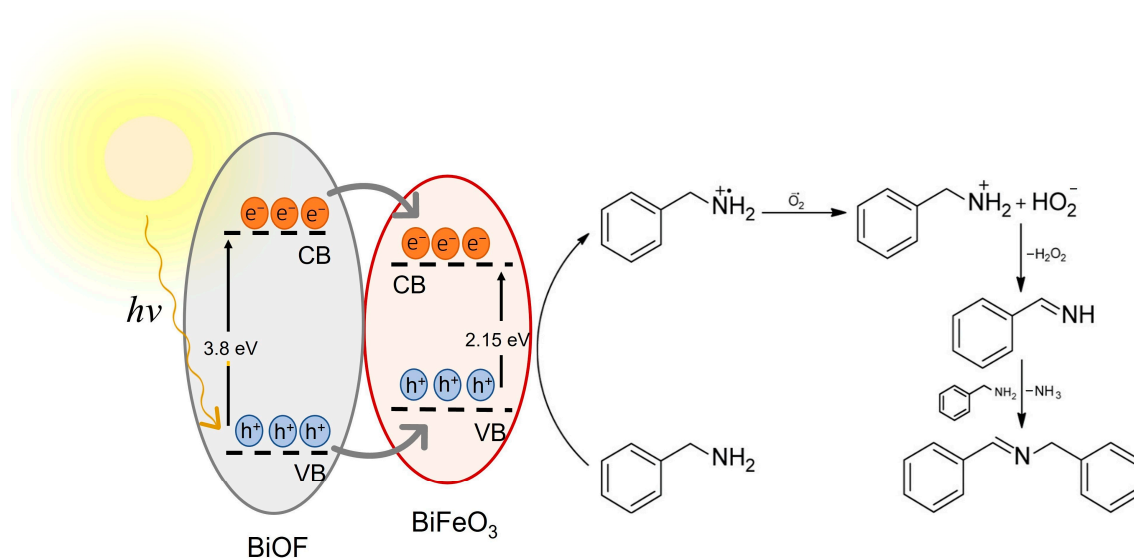
A plausible mechanism of the oxidative coupling of benzylamine is explained in Scheme 2. The process happens through an O_2^- mediated pathway when the photoexcited electron of the photocatalyst first rises to the conduction band (CB) upon radiation. It then reacts with atmospheric molecular oxygen to produce an O_2^- radical, which was previously confirmed using electron spin resonance (EPR) measurements [36–38]. An aminium radical cation intermediate is then formed by oxidized benzylamine by the photoinduced hole in the valence band (VB). Hydrogen-atom abstraction from the O_2^- radical then occurs at this radical cation, producing phenylmethanamine ($\text{Ph}-\text{CH}_2-\text{NH}_2$), and, thus, forming $\text{Ph}-$

CH=NH and H₂O₂ [36]. H₂O₂ is then dissociated to \cdot OH radicals, which act as a supporting material for benzylamine oxidation to the produced imine that finally reacts with another free benzylamine to produce the *N*-benzylidenebenzylamine product, liberating ammonia.

Table 2. Photocatalytic activities under different control conditions.

Entry	Control Conditions	Conversion Yield (%)
I	5 mg BiOF/BiFeO ₃ composite, light, solvent	80
II	BiOF/BiFeO ₃ composite, no solvent	13
III	BiFeO ₃ , no solvent	Nil
IV	BiOF, no solvent	7
V	BiOF/BiFeO ₃ composite, no light, no heat	Nil
VI	BiOF/BiFeO ₃ composite, heat, no light	2
VII	Heat, no light, no BiOF/BiFeO ₃ composite	Nil
VIII	Light, no BiOF/BiFeO ₃ composite	Nil

Reaction optimum conditions: 0.5 mmol (51 μ L) benzylamine, 0.16, 0.02, and 0.009 mmol (5 mg) of BiFeO₃, BiOF, and BiOF/BiFeO₃ composite, respectively; open air; irradiated for 24 h.



Scheme 2. Proposed mechanism of benzylamine coupling over reported photocatalyst.

4. Conclusions

In this study, benzylamine was photocatalytically coupled to *N*-benzylidenebenzylamine using the newly synthesized BiOF/BiFeO₃ composite photocatalyst, which showed a high conversion yield of 80% compared to other materials. The composite's construction was proven by multiple characterization methods, including XRD, DRS, SEM, EDX, and FT-IR. According to the measured band gaps, the BiOF/BiFeO₃ composite exhibited a lower band gap compared to BiOF (3.5 eV vs. 3.8 eV), which can be successfully employed as a photocatalyst in the UV region. The reported synthesis procedure provides an easy, eco-friendly, and low-cost route for developing various active materials for photocatalytic applications.

Supplementary Materials: The following supporting information can be downloaded at: <https://www.mdpi.com/article/10.3390/photochem3010012/s1>, Figure S1: Matched X-ray spectroscopy of the BiOF using Match!3 software (version 3.0). Figure S2: Matched X-ray spectroscopy of the BiFeO₃ using Match!3 software (version 3.0); Figure S3: EDX elemental analysis of BiOF; Figure S4: EDX elemental analysis of BiFeO₃; Figure S5: EDX elemental analysis of BiOF/ BiFeO₃ composite; Table S1: Weight and atomic percentages of BiOF; Table S2: Weight and atomic percentages of BiFeO₃; Table S3: Weight and atomic percentages of BiOF/ BiFeO₃ composite; Figure S6: Spectra of *N*-benzylidenebenzylamine product using ¹H-NMR (A) and ¹³C-NMR (B); Figure S7: FTIR spectrum of *N*-benzylidenebenzylamine.

Author Contributions: Conceptualization, A.A. and A.S.A.; methodology, A.S.A., R.H.A. and L.A.S.; software, A.S.A., R.H.A. and L.A.S.; validation, A.A.; formal analysis, A.S.A., R.H.A. and L.A.S.; investigation, A.S.A., R.H.A., L.A.S., A.E., D.A., Z.K., H.Z. and R.E.; resources, A.A.; data curation, A.S.A., R.H.A., L.A.S. and A.A.; writing—original draft preparation, A.S.A., R.H.A., L.A.S. and A.A.; writing—review and editing, A.A.; visualization, A.S.A.; supervision, A.A.; project administration, A.A.; funding acquisition, A.A. All authors have read and agreed to the published version of the manuscript.

Funding: This research was funded by United Arab Emirates University, grant no. 31R238 and SURE Plus 2022 project, grant code G00003232.

Data Availability Statement: The datasets generated during and/or analysed during the current study are available from the corresponding author on reasonable request.

Acknowledgments: This work was financially supported by the National Water and Energy Center and by the United Arab Emirates University.

Conflicts of Interest: All authors certify that the submission is original work and is not under review at any other publication.

References

- Smith, R.T.; Achenbach, G.D.; Gerson, R.; James, W.J. Dielectric Properties of Solid Solutions of BiFeO₃ with Pb(Ti, Zr)O₃ at High Temperature and High Frequency. *J. Appl. Phys.* **1968**, *39*, 70–74. [\[CrossRef\]](#)
- Bhide, V.G.; Multani, M.S. Mössbauer Effect in Ferroelectric-Antiferromagnetic BiFeO₃. *Solid State Commun.* **1965**, *3*, 271–274. [\[CrossRef\]](#)
- Béa, H.; Bibes, M.; Cherifi, S.; Nolting, F.; Warot-Fonrose, B.; Fusil, S.; Herranz, G.; Deranlot, C.; Jacquet, E.; Bouzehouane, K.; et al. Tunnel Magnetoresistance and Robust Room Temperature Exchange Bias with Multiferroic BiFeO₃ Epitaxial Thin Films. *Appl. Phys. Lett.* **2006**, *89*, 3–6. [\[CrossRef\]](#)
- Béa, H.; Bibes, M.; Sirena, M.; Herranz, G.; Bouzehouane, K.; Jacquet, E.; Fusil, S.; Paruch, P.; Dawber, M.; Contour, J.P.; et al. Combining Half-Metals and Multiferroics into Epitaxial Heterostructures for Spintronics. *Appl. Phys. Lett.* **2006**, *88*, 4–7.
- Tong, T.; Chen, J.; Jin, D.; Cheng, J. Preparation and Gas Sensing Characteristics of BiFeO₃ Crystallites. *Mater. Lett.* **2017**, *197*, 160–162. [\[CrossRef\]](#)
- Das, S.; Rana, S.; Mursalin, S.M.; Rana, P.; Sen, A. Sonochemically Prepared Nanosized BiFeO₃ as Novel SO₂ Sensor. *Sensors Actuators B Chem.* **2015**, *218*, 122–127. [\[CrossRef\]](#)
- Gao, F.; Chen, X.Y.; Yin, K.B.; Dong, S.; Ren, Z.F.; Yuan, F.; Yu, T.; Zou, Z.G.; Liu, J.-M. Visible-Light Photocatalytic Properties of Weak Magnetic BiFeO₃ Nanoparticles. *Adv. Mater.* **2007**, *19*, 2889–2892. [\[CrossRef\]](#)
- Xian, T.; Yang, H.; Dai, J.F.; Wei, Z.Q.; Ma, J.Y.; Feng, W.J. Photocatalytic Properties of BiFeO₃ Nanoparticles with Different Sizes. *Mater. Lett.* **2011**, *65*, 1573–1575. [\[CrossRef\]](#)
- Mushtaq, F.; Chen, X.; Hoop, M.; Torlakcik, H.; Pellicer, E.; Sort, J.; Gattinoni, C.; Nelson, B.J.; Pané, S. Piezoelectrically Enhanced Photocatalysis with BiFeO₃ Nanostructures for Efficient Water Remediation. *iScience* **2018**, *4*, 236–246. [\[CrossRef\]](#)
- Sando, D.; Yang, Y.; Bousquet, E.; Carrétéro, C.; Garcia, V.; Fusil, S.; Dolfi, D.; Barthélémy, A.; Ghosez, P.; Bellaiche, L.; et al. Large Elasto-Optic Effect and Reversible Electrochromism in Multiferroic BiFeO₃. *Nat. Commun.* **2016**, *7*, 10718. [\[CrossRef\]](#)
- Chu, S.H.; Singh, D.J.; Wang, J.; Li, E.-P.; Ong, K.P. High Optical Performance and Practicality of Active Plasmonic Devices Based on Rhombohedral BiFeO₃. *Laser Photonics Rev.* **2012**, *6*, 684–689. [\[CrossRef\]](#)
- Zeches, R.J.; Rossell, M.D.; Zhang, J.X.; Hatt, A.J.; He, Q.; Yang, C.-H.; Kumar, A.; Wang, C.H.; Melville, A.; Adamo, C.; et al. A Strain-Driven Morphotropic Phase Boundary in BiFeO₃. *Science* **2009**, *326*, 977–980. [\[CrossRef\]](#) [\[PubMed\]](#)
- Kumar, A.; Rai, R.C.; Podraza, N.J.; Denev, S.; Ramirez, M.; Chu, Y.H.; Martin, L.W.; Ihlefeld, J.; Heeg, T.; Schubert, J.; et al. Linear and Nonlinear Optical Properties of BiFeO₃. *Appl. Phys. Lett.* **2008**, *92*, 67–70. [\[CrossRef\]](#)
- Li, S.; Lin, Y.-H.; Zhang, B.-P.; Wang, Y.; Nan, C.-W. Controlled Fabrication of BiFeO₃ Uniform Microcrystals and Their Magnetic and Photocatalytic Behaviors. *J. Phys. Chem. C* **2010**, *114*, 2903–2908. [\[CrossRef\]](#)
- Alzard, R.H.; Siddig, L.A.; Alhatti, N.; Abdallah, I.; Albabri, L.; Alblooshi, A.; Alzamly, A. Titania Derived from NH₂-MIL-125(Ti) Metal—Organic Framework for Selective Photocatalytic Conversion of CO₂ to Propylene Carbonate. *Comments Inorg. Chem.* **2022**, *43*, 1–15. [\[CrossRef\]](#)
- Lam, S.-M.; Sin, J.-C.; Mohamed, A.R. A Newly Emerging Visible Light-Responsive BiFeO₃ Perovskite for Photocatalytic Applications: A Mini Review. *Mater. Res. Bull.* **2017**, *90*, 15–30. [\[CrossRef\]](#)
- Rouhani, Z.; Karimi-Sabet, J.; Mehdi-pourghazi, M.; Hadi, A.; Dastbaz, A. Response Surface Optimization of Hydrothermal Synthesis of Bismuth Ferrite Nanoparticles under Supercritical Water Conditions: Application for Photocatalytic Degradation of Tetracycline. *Environ. Nanotechnol. Monit. Manag.* **2019**, *11*, 100198. [\[CrossRef\]](#)
- Haruna, A.; Abdulkadir, I.; Idris, S.O. Photocatalytic Activity and Doping Effects of BiFeO₃ Nanoparticles in Model Organic Dyes. *Heliyon* **2020**, *6*, e03237. [\[CrossRef\]](#)

19. Kumar, V.; Soam, A.; Sahoo, P.K.; Panda, H.S. Enhancement of Electrochemical Properties of Carbon Solution Doped Bismuth Ferrite for Supercapacitor Application. *Mater. Today Proc.* **2021**, *41*, 165–171. [\[CrossRef\]](#)
20. Sankar Ganesh, R.; Sharma, S.K.; Sankar, S.; Divyapriya, B.; Durgadevi, E.; Raji, P.; Ponnusamy, S.; Muthamizhchelvan, C.; Hayakawa, Y.; Kim, D.Y. Microstructure, Structural, Optical and Piezoelectric Properties of BiFeO₃ Nanopowder Synthesized from Sol-Gel. *Curr. Appl. Phys.* **2017**, *17*, 409–416. [\[CrossRef\]](#)
21. Asahi, R.; Morikawa, T.; Ohwaki, T.; Aoki, K.; Taga, Y. Visible-Light Photocatalysis in Nitrogen-Doped Titanium Oxides. *Science*. **2001**, *293*, 269–271. [\[CrossRef\]](#) [\[PubMed\]](#)
22. Cho, C.M.; Noh, J.H.; Cho, I.S.; An, J.S.; Hong, K.S.; Kim, J.Y. Low-Temperature Hydrothermal Synthesis of Pure BiFeO₃ Nanopowders Using Triethanolamine and Their Applications as Visible-Light Photocatalysts. *J. Am. Ceram. Soc.* **2008**, *91*, 3753–3755. [\[CrossRef\]](#)
23. Sharif, M.K.; Khan, M.A.; Hussain, A.; Iqbal, F.; Shakir, I.; Murtaza, G.; Akhtar, M.N.; Ahmad, M.; Warsi, M.F. Synthesis and Characterization of Zr and Mg Doped BiFeO₃ Nanocrystalline Multiferroics via Micro Emulsion Route. *J. Alloys Compd.* **2016**, *667*, 329–340. [\[CrossRef\]](#)
24. Shami, M.Y.; Awan, M.S.; Anis-ur-Rehman, M. Phase Pure Synthesis of BiFeO₃ Nanopowders Using Diverse Precursor via Co-Precipitation Method. *J. Alloys Compd.* **2011**, *509*, 10139–10144. [\[CrossRef\]](#)
25. Azam, A.; Jawad, A.; Ahmed, A.S.; Chaman, M.; Naqvi, A.H. Structural, Optical and Transport Properties of Al₃⁺ Doped BiFeO₃ Nanopowder Synthesized by Solution Combustion Method. *J. Alloys Compd.* **2011**, *509*, 2909–2913. [\[CrossRef\]](#)
26. Wani, W.A.; Kundu, S.; Ramaswamy, K.; Venkataraman, B.H. Optimizing Phase Formation of BiFeO₃ and Mn-Doped BiFeO₃ Nanoceramics via Thermal Treatment Using Citrate Precursor Method. *SN Appl. Sci.* **2020**, *2*, 1969. [\[CrossRef\]](#)
27. Haruna, A.; Abdulkadir, I.; Idris, S.O. Synthesis, Characterization and Photocatalytic Properties of Bi_{0.85}-XMXBa_{0.15}FeO₃ (M = Na and K, X = 0, 0.1) Perovskite-like Nanoparticles Using the Sol-Gel Method. *J. King Saud Univ.-Sci.* **2020**, *32*, 896–903. [\[CrossRef\]](#)
28. Alzamly, A.; Bakiro, M.; Ahmed, S.H.; Sallabi, S.M.; Al Ajeil, R.A.; Alawadhi, S.A.; Selem, H.A.; Al Meshayei, S.S.M.; Khaleel, A.; Al-Shamsi, N.; et al. Construction of BiOF/BiOI Nanocomposites with Tunable Band Gaps as Efficient Visible-Light Photocatalysts. *J. Photochem. Photobiol. A Chem.* **2019**, *375*, 30–39. [\[CrossRef\]](#)
29. Li, H.; Yu, K.; Lei, X.; Guo, B.; Fu, H.; Zhu, Z. Hydrothermal Synthesis of Novel MoS₂/BiVO₄ Hetero-Nanoflowers with Enhanced Photocatalytic Activity and a Mechanism Investigation. *J. Phys. Chem. C* **2015**, *119*, 22681–22689. [\[CrossRef\]](#)
30. Dai, G.; Liu, S.; Liang, Y.; Luo, T. Synthesis and Enhanced Photoelectrocatalytic Activity of P-n Junction Co₃O₄/TiO₂ Nanotube Arrays. *Appl. Surf. Sci.* **2013**, *264*, 157–161. [\[CrossRef\]](#)
31. Zhang, J.; Qiao, S.Z.; Qi, L.; Yu, J. Fabrication of NiS Modified CdS Nanorod P-n Junction Photocatalysts with Enhanced Visible-Light Photocatalytic H₂-Production Activity. *Phys. Chem. Chem. Phys.* **2013**, *15*, 12088–12094. [\[CrossRef\]](#) [\[PubMed\]](#)
32. Zhou, M.; Yu, J.; Liu, S.; Zhai, P.; Jiang, L. Effects of Calcination Temperatures on Photocatalytic Activity of SnO₂/TiO₂ Composite Films Prepared by an EPD Method. *J. Hazard. Mater.* **2008**, *154*, 1141–1148. [\[CrossRef\]](#) [\[PubMed\]](#)
33. Alzard, R.H.; Siddig, L.A.; Abdelhamid, S.A.; Alzamly, A. Visible-Light-Driven Photocatalytic Coupling of Neat Benzylamine over a Bi-Ellagate Metal–Organic Framework. *ACS Omega* **2022**, *7*, 36689–36696. [\[CrossRef\]](#) [\[PubMed\]](#)
34. Guo, J.; Ma, D.; Sun, F.; Zhuang, G.; Wang, Q.; Al-Enizi, A.M.; Nafady, A.; Ma, S. Substituent Engineering in G-C₃N₄/COF Heterojunctions for Rapid Charge Separation and High Photo-Redox Activity. *Sci. China Chem.* **2022**, *65*, 1704–1709. [\[CrossRef\]](#)
35. Fu, Y.; Tan, M.; Guo, Z.; Hao, D.; Xu, Y.; Du, H.; Zhang, C.; Guo, J.; Li, Q.; Wang, Q. Fabrication of Wide-Spectra-Responsive NA/NH₂-MIL-125(Ti) with Boosted Activity for Cr(VI) Reduction and Antibacterial Effects. *Chem. Eng. J.* **2023**, *452*, 139417. [\[CrossRef\]](#)
36. Li, J.; Chang, B.; Zhao, H.; Meng, Q.; Li, M.; Han, Q. Visible-Light-Responsive Polyoxometalate-Based Metal–Organic Framework for Highly Efficient Photocatalytic Oxidative Coupling of Amines. *J. Mater. Sci.* **2021**, *56*, 6676–6688. [\[CrossRef\]](#)
37. Su, F.; Mathew, S.C.; Möhlmann, L.; Antonietti, M.; Wang, X.; Blechert, S. Aerobic Oxidative Coupling of Amines by Carbon Nitride Photocatalysis with Visible Light. *Angew. Chem. Int. Ed.* **2011**, *50*, 657–660. [\[CrossRef\]](#)
38. Zheng, S.; Du, H.; Yang, L.; Tan, M.; Li, N.; Fu, Y.; Hao, D.; Wang, Q. PDINH Bridged NH₂-UiO-66(Zr) Z-Scheme Heterojunction for Promoted Photocatalytic Cr(VI) Reduction and Antibacterial Activity. *J. Hazard. Mater.* **2023**, *447*, 130849. [\[CrossRef\]](#)

Disclaimer/Publisher's Note: The statements, opinions and data contained in all publications are solely those of the individual author(s) and contributor(s) and not of MDPI and/or the editor(s). MDPI and/or the editor(s) disclaim responsibility for any injury to people or property resulting from any ideas, methods, instructions or products referred to in the content.